

TSJNet: A Multi-modality Target and Semantic Awareness Joint-driven Image Fusion Network

Yuchan Jie*, Yushen Xu*, Xiaosong Li†, Haishu Tan

School of Physics and Optoelectronic Engineering, Foshan University, Foshan, China

jyc981214@163.com, yushenxu01@gmail.com, lixiaosong@buaa.edu.cn, tanhaishu@fosu.edu.cn

Abstract

Multi-modality image fusion involves integrating complementary information from different modalities into a single image. Current methods primarily focus on enhancing image fusion with a single advanced task such as incorporating semantic or object-related information into the fusion process. This method creates challenges in achieving multiple objectives simultaneously. We introduce a target and semantic awareness joint-driven fusion network called TSJNet. TSJNet comprises fusion, detection, and segmentation subnetworks arranged in a series structure. It leverages object and semantically relevant information derived from dual high-level tasks to guide the fusion network. Additionally, We propose a local significant feature extraction module with a double parallel branch structure to fully capture the fine-grained features of cross-modal images and foster interaction among modalities, targets, and segmentation information. We conducted extensive experiments on four publicly available datasets (MSRS, M^3FD , RoadScene, and LLVIP). The results demonstrate that TSJNet can generate visually pleasing fused results, achieving an average increase of 2.84% and 7.47% in object detection and segmentation mAP @0.5 and mIoU, respectively, compared to the state-of-the-art methods.

1. Introduction

Multisensor integration systems are indispensable in intelligent technologies, including unmanned aerial vehicle (UAV) precision combat and automatic driving. As sensor manufacturing improves, the comprehensive use of multi-modality images for complex real-world scene analysis is becoming increasingly important. Visible light and infrared sensors, which are widely used, have their own limitations. While visible light sensors struggle to effectively highlight targets under low-light conditions, infrared sensors, unaf-

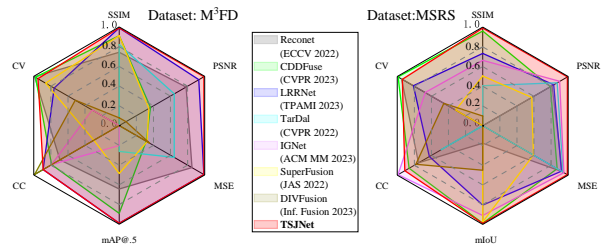


Figure 1. Comparison of results with SOTA methods on the M^3FD [15] and MSRS [32] datasets. The radar map highlights the superiority of the TSJNet.

ected by this issue, offer low scene resolution and capture texture details poorly. Fortunately, multi-modality image fusion (MMIF) can address these issues by synthesizing data from multi-sources, compensating for the information loss in single-modal data, and enhancing the understanding and perception of both human and machine vision. Furthermore, MMIF is expected to generate more accurate representations of targets and scenes, positively impacting downstream tasks such as semantic segmentation [31] and object detection [29].

Recently, proficient feature extraction abilities of deep learning (DL) have led to the appearance of DL-based MMIF approaches. However, these approaches have two problems. First, the modality gap is too wide, resulting in the inability to efficiently extract cross-modal features. Second, many methods overlook the mutual reinforcement between downstream tasks and the fusion process. Our research introduces a more rational framework designed to facilitate the reciprocal enhancement of MMIF, image segmentation, and object detection.

For the first problem, insufficient attention has been paid to the internal structure of information delivery in some networks [47], leading to the loss of important details. Therefore, considering the interactive and independent features to improve the performance of feature extraction is one key to our model. Taking infrared and visible image fusion

*equal contribution

†corresponding author

(IVIF) as an example, the two modal images acquire the same scene, so basic information, such as the large-scale contour of the object, belongs to interactive features. The thermal radiation of the infrared image and the texture edge of the visible image are independent features. Adequate extraction of bimodal image features allows full utilization of overall and local details.

For the second problem. A valuable MMIF model generates high-quality images in real-life scenes and facilitates downstream tasks. Although some approaches [1, 5, 14, 22] exhibit good fusion performance, they hardly consider achieving mutual gain between downstream tasks and image fusion, which is essential for practical computer vision applications. These fusion models emphasize determining commonalities among different modal images but ignore the differences between significant object presentation, background, and semantic information. Interestingly, several recent studies [29, 31, 48] established a connection between image fusion and object detection, or semantic segmentation. They used an additional semantic segmentation or object detection networks to embed the necessary semantic or detection information in the fusion network. However, there is no focus on the use of both to promote a fusion network. To fill this gap, the most crucial aspect of our model is establishing a MMIF framework driven by segmentation and object detection perception simultaneously, thus allowing the proposed model to significantly improve MMIF tasks.

Notably, common structures of fusion networks leverage inductive constraints and are limited in mining and integrating global contextual information within and across modalities. Nevertheless, attention mechanisms can extract extensive interactions between contexts and model dependencies without considering their distance in the input or output sequence [36], which has demonstrated encouraging results for multiple vision-related challenges [3]. Therefore, the aim is to establish a fusion model that combines the advantages of the CNN and attention mechanism to improve MMIF performance.

To accomplish these objectives, we propose a multi-feature learning multi-modality image fusion network with drivers of segmentation and detection. This network includes three parts: firstly, an auto-encoder (AE) module is employed based on residual networks with split-attention (ResNeSt) [46] for interactive feature extraction. Furthermore, AE-based networks demonstrate good reconstruction performance [9]. Secondly, a feature fusion module based on the proposed local significant feature extraction model (LSM). Thirdly, common semantic segmentation and object detection networks are introduced to navigate the refinement of fusion features and improve the overall fusion performance. Fig. 1 shows that TSJNet has the best fusion performance compared with seven state-of-the-art (SOTA)

methods.

Our contributions are as follows:

- We propose a MMIF network driven by both detection and segmentation tasks. Different from existing fusion methods, this is the first time that two high-level tasks have been included in the fusion network simultaneously.
- We develop the LSM with parallel double branches to fully extract local details, thereby increasing the fusion network’s flexibility and improving the integration of complementary attribute features.
- We conduct image fusion, semantic segmentation, and detection experiments using the proposed TSJNet on the MSRS, M³FD, LLVIP, and RoadScene datasets. Compared to the seven advanced fusion methods, our model has significant superiorities.

2. Related works

2.1. Multi-modal image fusion

Over the past few years, a myriad of DL-based MMIF approaches have been proposed, and can be primarily categorized into four types: convolutional neural network (CNN)- [16, 39, 40], generative adversarial network (GAN)- [15, 20, 21, 26], diffusion model- [44, 50], and auto-encoder (AE)-based methods [12, 24, 47, 49]. Although the remarkable development of DL for low-level vision tasks can be attributed to the strong nonlinear fitting capacity exhibited by multi-layer neural networks, less attention has been paid to whether high-level tasks can be effectively integrated with low-level vision tasks. Cross-task learning allows consolidated models to meet challenges stemming from the scarcity of training data and the absence of ground truth [45]. Liu et al. [19] created a deep-learning model for a dual-task hierarchy to improve the mutual benefits of semantic perception and image fusion tasks. To focus on both the target-related information and pixel-level details in an image, Sun et al. [29] employed insights gained from object detection networks to direct MMIF. To explore the potential of image-level fusion for semantically driven methods, Tang et al. [34] established an image-fusion network constrained by scene authenticity and incremental semantic integration. In addition, to minimize the effect of different modal image alignment accuracies on fusion, Xu et al. [42] utilized the response of image fusion to enhance registration accuracy. Wang et al. [38] proposed a paradigm for misaligned infrared and visible light images using intermodal generation and registration.

3. The proposed TSJNet

3.1. Motivation

Application domains, such as autonomous driving and multi-modality image processing, require object detection

and semantic segmentation algorithms to achieve accurate scene understanding and object recognition. MMIF can satisfy the requirements of real-world applications that operate around the clock. Although most recent studies [22, 35, 42] have emphasized enhancing the details or contrast of images, they have often overlooked the effects of image fusion on downstream tasks. The purpose of semantic segmentation is to distinguish between regions with different semantic properties in an image, whereas object detection requires the location and recognition of objects. Undoubtedly, capturing advanced semantics and target information is more critical than solely focusing on fine-grained image details. Therefore, we propose a fusion model that benefits from semantic and object-related information.

3.2. Problem formulation

To facilitate the explanation, the overall algorithm is visualized in Fig. 2, and the algorithm is described in detail below, using IVIF as an example. The prevalent approach to image detection, segmentation, or fusion tasks involves creating a neural network and making the most of it to determine an ideal set of parameters. To this end, assuming that the infrared, visible, and fused images have dimensions of $p \times q$, we represent them as individual vectors $\mathbf{x}, \mathbf{y}, \mathbf{u} \in \mathbb{R}^{p \times q \times l}$. The l is the number of channels. The optimization framework is defined as follows:

$$\min_{\theta_t} f(t, \mathcal{X}(\mathbf{y}; \theta_t)) \quad (1)$$

where $f(\cdot)$ denotes the matching term, and t represents the result produced by the task-specific network \mathcal{X} with the adjustable parameters denoted as θ_t .

To produce a fused image that is visually pleasing while also obtaining precise scene segmentation and object detection outcomes, we integrated the three tasks into a unified objective, which can be represented as:

$$\min_{\omega_u, \omega_d, \omega_s} f_u(\mathbf{u}, \Phi(\mathbf{X}, \omega_u)) + f_d(\mathbf{d}, \Psi(\mathbf{Y}, \mathbf{u}, \omega_d)) + f_s(\mathbf{s}, \Theta(\mathbf{u}, \omega_s)) \quad (2)$$

where \mathbf{u} , \mathbf{d} , and \mathbf{s} are the fusion result, detection object, and segmentation map, which are generated by the fusion network Φ , detection network Ψ and segmentation network Θ respectively.

Comprehensive network framework. Fig. 3 depicts the TSJNet. Our model embodies the dual-drive principle, uniting subnetworks for image fusion; DeepLabV3+ with ResNet101 [4] and Faster R-CNN [27] are employed as the baseline detection and segmentation models to provide object detection and segmentation information.

3.3. Details of TSJNet

We established a set of symbols to enhance the precision of the formulation. We represent the paired input images,

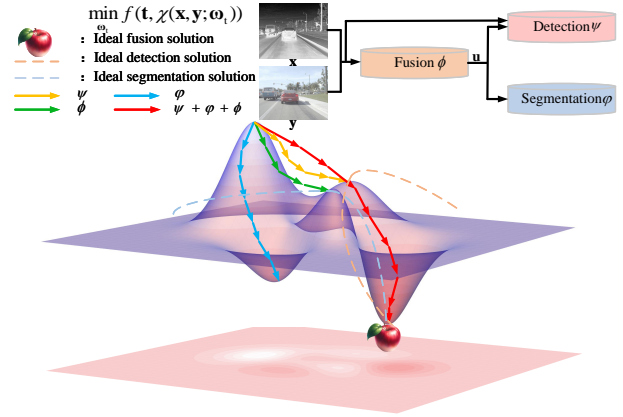


Figure 2. Fusion gradient optimization process.

specifically the infrared and visible images, as $\mathbf{I} \in \mathbb{R}^{p \times q}$ and $\mathbf{V} \in \mathbb{R}^{p \times q \times 3}$, respectively.

3.3.1 Encoder

The encoder is comprised of two parts: the ResNeSt [49] block based encoder and the convolutional layer-based feature refinement block.

Base ResNeSt Encoder (BRE). The encoder extracts the hierarchical features F_I^B, F_V^B from \mathbf{I}, \mathbf{V} , that is,

$$F_i^B = BRE(\mathbf{I}), \quad F_v^B = BRE(\mathbf{V}) \quad (3)$$

The split-attention block in ResNeSt harnesses the synergistic advantages offered by polyroute depiction and feature map attention, which enhances feature representations. This allows the model to adaptively tune the feature map, focusing on key channels and spatial locations to capture the complex interactions between different features. Therefore, we employed ResNeSt as part of the encoder to enhance its ability to facilitate complex cross-feature interactions between the infrared and visible images.

3.3.2 Fusion Layer

LSM. Because the fine-grained features of different modal images are significantly different, a feature extraction block with a side-by-side two-branch structure is proposed to extract significant local information during cross-modal feature extraction. The LSM is composed of a neighborhood attention transformer (NAT) [7] based on a sliding window and the proposed detail salience module (DSM).

The neighborhood attention (NA) of the NAT localizes the attention scope of each pixel to its closest neighbors, converges to self-attention with an increase in scope, maintains translation invariance, and mitigates the complexity and localization problems of self-attention mechanisms in

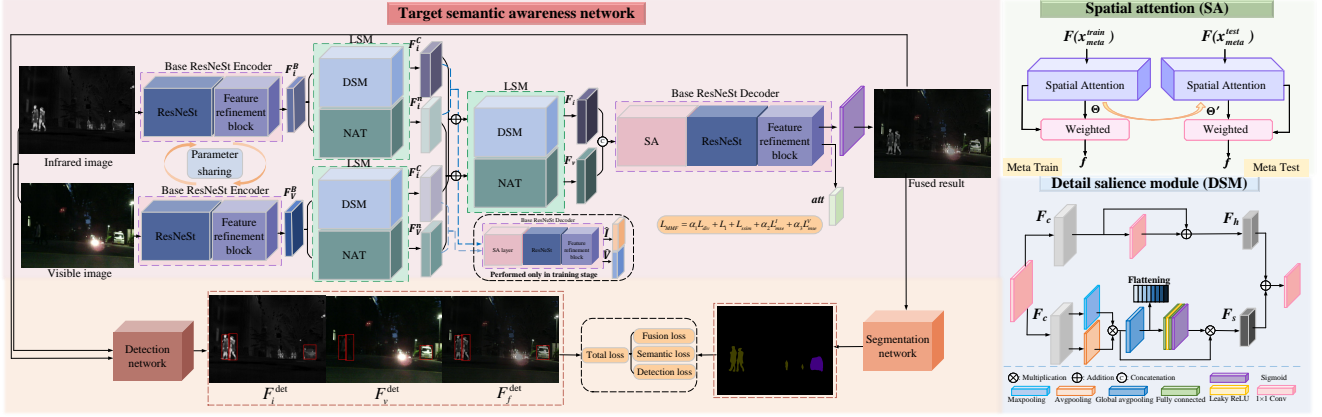


Figure 3. Framework of the proposed TSJNet with dual drivers of segmentation and detection.

visual tasks. Moreover, it has higher efficiency than stand-alone self-attention [25] and Swin Transformer [18].

The DSM was designed to enhance the representation of structural attributes of our modal. F_c can be obtained after a convolution layer, and two distinct feature-extraction branches are combined to form a feature-extraction module. Motivated by [14], one branch simultaneously performs average pooling and max pooling to synchronize the extraction of details with the global information. After dual pooling, the features are further expanded using global average pooling. Subsequently, the weights of the different channels are computed by allocating two fully connected layers and a sigmoid layer, which enhances the significance of the feature depiction. Summing this branch with another residual branch can extract more salient information from the infrared image and structural information from the visible image. The expressions are as follows:

$$\{F_i^d, F_i^n\} = L(F_i^B), \quad \{F_v^d, F_v^n\} = L(F_v^B) \quad (4)$$

where F_i^d and F_i^n are the local and salient features of I , and F_v^d and F_v^n are for V ; $L(\cdot)$ represents the LSM.

After the corresponding features are fused, we sum the corresponding detail features of I and V input them into DSM and NAT to obtain the pre-fused features of the infrared and visible images F_d and F_n , respectively.

$$F_d = D(F_i^d + F_v^d), \quad F_n = N(F_i^n + F_v^n) \quad (5)$$

where F_d and F_n are the fused salient and local features, respectively; $D(\cdot)$ represents the DSM, $N(\cdot)$ represents the NAT.

3.3.3 Decoder

Base ResNeSt Decoder (BRD). We introduce a spatial attention module based on meta-learning to enhance the model's generalization and transfer learning capabilities

and promote the positive transmission of cross-modal information across various datasets. The local and salient features abstracted by the fusion layer are added as inputs for $BRD(\cdot)$. Using cross modalities as inputs, we maintain the uniformity of the decoder structure with BRE by utilizing ResNeSt as the core component. The fused result is obtained using the decoder and can be expressed as follows:

$$F = BRD(F_d + F_n) \quad (6)$$

where F denotes the fused result.

4. Loss function

TSJNet aims to enhance the visual quality of the fused results and serve downstream tasks well. To achieve this, we use the location-awareness capability and scale invariance of the detection model, semantic information extraction capability, and pixel-level refinement of the segmentation model. Therefore, the detection loss \mathcal{L}_{Det} , segmentation loss \mathcal{L}_{Seg} and multifaceted fusion loss (MFFLoss) \mathcal{L}_{MFF} are well designed to guide the optimization of our network, which is the most significant innovation of TSJNet. The loss function formulation in [27] is introduced as the detection loss, and the cross-entropy loss function is introduced as the segmentation loss. The precise formulation of the fusion loss can be presented as:

$$\mathcal{L}_{all} = \mathcal{L}_{MFF} + \mathcal{L}_{Det} + \mathcal{L}_{Seg} \quad (7)$$

where \mathcal{L}_{all} denotes the total loss.

4.1. MultiFacet Fusion Loss

In upstream and downstream tasks, the image quality directly affects the model's performance. For object detection, the preservation of entity edges and feature information is crucial to accurately localize and identify different objects. The design of the MFFLoss is aimed at making

fused images more suitable for subsequent object detection and semantic segmentation.

The semantic segmentation task requires every pixel of the image to be correctly classified, which requires additional visual and contextual information. MFFLoss emphasizes the preservation of the global structure through the loss of the structural similarity metric, $\mathcal{L}_{\text{ssim}}$, which is crucial for pixel-level classification in semantic segmentation, as shown in Eqs.8.

$$\mathcal{L}_{\text{ssim}} = \frac{1}{2} (1 - \text{ssim}(\mathbf{F}, \mathbf{I})) + \frac{1}{2} (1 - \text{ssim}(\mathbf{F}, \mathbf{V})) \quad (8)$$

where $\text{ssim}(\cdot)$ calculates the structural similarity.

Obtaining high accuracy and diverse image content can bridge the gap between upstream and downstream tasks. The diversity loss \mathcal{L}_{div} [2] was introduced to maintain the stability and flexibility of the fusion model for independent and cross-modal feature extraction by encouraging the attentional mechanism to avoid overconcentration, which is crucial for dealing with the detection of multiple targets and categories in complex scenes, as presented in Eq.9.

$$\mathcal{L}_{\text{div}} = -\frac{1}{m} \sum_{i=1}^m \left(1 - \max_j att_{i,j} \right) + \frac{1}{mn} \sum_{i=1}^m \sum_{j=1}^n att_{i,j} \quad (9)$$

where att is the attentional weight matrix generated in the decoder training phase, m and n are the number of rows and columns, respectively.

Ultimately, The aim of our model can be presented as follows:

$$\mathcal{L}_{\text{MFF}} = \alpha_1 \mathcal{L}_{\text{div}} + \mathcal{L}_{\text{ssim}} + \alpha_2 \mathcal{L}'_{\text{mse}} + \alpha_3 \mathcal{L}''_{\text{mse}} \quad (10)$$

where $\mathcal{L}'_{\text{mse}} = \|\mathbf{I} - \tilde{\mathbf{I}}\|_2^2$ and $\mathcal{L}''_{\text{mse}} = \|\mathbf{V} - \tilde{\mathbf{V}}\|_2^2$, and α_1 , α_2 , and α_3 are the tuning parameters.

4.2. Detection Loss

The infrared, visible, and fused results are input to the detection network separately for calculating the detection loss based on the ground truth and respective predictions. We represent the detection loss for the \mathbf{I} , \mathbf{V} , and \mathbf{F} as $\mathcal{L}_{\text{det}}^I$, $\mathcal{L}_{\text{det}}^V$, and $\mathcal{L}_{\text{det}}^F$, respectively. The detection loss \mathcal{L}_{Det} can be denoted as follows,

$$\mathcal{L}_{\text{Det}} = \mathcal{L}_{\text{det}}^I + \mathcal{L}_{\text{det}}^V + \mathcal{L}_{\text{det}}^F \quad (11)$$

To improve the generalization capability and computational efficiency of our model, the classification loss was removed from original object detection loss [27], retaining only the regression loss [29]. Furthermore, the detection loss functions only when the fusion network needs to be modified. Taking a fusion-detection network as an example,

$$\mathcal{L}_{\text{det}}^F(u, t^u, v) = [u \geq 1] \mathcal{L}_{\text{det}}^F(t^u, v) \quad (12)$$

where u is the ground truth class, t^u is the the predicted outcome of the bounding box, and v is the regression goal of the ground truth bounding box. The Iverson bracket indicator function $[u \geq 1]$ is 1 when $u \geq 1$ is satisfied, and 0 otherwise. We label the background class as $u = 0$. $\mathcal{L}_{\text{reg}}^F$ is the L1 loss.

4.3. Semantic Loss

For fully enhancing the semantic information of the fusion results, DeepLabV3+ [4] was introduced into our model, and semantic loss was added to MFFLoss. The semantic loss can be represented as:

$$\mathcal{L}_{\text{seg}} = -\frac{1}{PQ} \sum_{p=1}^P \sum_{q=1}^Q \log \left(\frac{\exp(\hat{y}_{c_{p,q},p,q})}{\sum_{j=1}^C \exp(\hat{y}_{j,p,q})} \right) \quad (13)$$

where $c_{p,q}$ denotes the true class index at position (p, q) . $\hat{y}_{j,p,q}$ is the model's prediction of belonging to class j at position (p, q) in logits.

5. Experiment

5.1. Setup

5.1.1 Experimental Detail

Total experiments were conducted on a server with four RTX 3090 GPUs. Because chunking and resizing the image lead to a loss of semantic information and labeling failure, we used the original image size for training. There were 40 training epochs, and the batch size was set to two. We used the Adam optimization function with an initial learning rate of 0.001. When the value of the loss function did not progress three consecutive times, the learning rate was reduced by a factor of 0.1 times the original. We used the pre-trained Faster R-CNN with the ResNet-50 and FPN [27] models and a pre-trained DeepLabV3+ with the ResNet101 [4] model for object detection and semantic segmentation. The three adjustable parameters α_1 , α_2 , and α_3 in Eq.10 are taken as 0.1, 6, and 1, respectively. Moreover, a precision [23] strategy was applied during training to reduce memory usage.

5.1.2 Datasets, Metrics, and compared methods

Datasets: Four common benchmarks were simultaneously employed to validate our fusion model: i.e., MSRS [32], M³FD [15], Road Scene[41], and LLVIP [10]. Our network was trained on the MSRS dataset (1035 pairs) and tested on MSRS (362 pairs), M³FD (300 pairs), RoadScene (221 pairs), and LLVIP (3463 pairs), which were synthesized to validate the better generalization capability of our fusion network.

The LLVIP, M³FD, and RoadScene datasets lack semantic segmentation labels or object detection labels, which is

Table 1. Objective comparisons of different methods on MSRS, M³FD, RoadScene, and LLVIP datasets. The top three values are marked in red, green, and blue.

MSRS [32] IVIF dataset							M ³ FD [15] IVIF dataset						
Method	SSIM \uparrow	PSNR \uparrow	MSE \downarrow	VIF \uparrow	CC \uparrow	CV \downarrow	Method	SSIM \uparrow	PSNR \uparrow	MSE \downarrow	VIF \uparrow	CC \uparrow	CV \downarrow
ReC [8]	0.30	16.38	2005.55	0.31	0.56	319.06	ReC [8]	0.67	14.11	2989.60	0.33	0.51	496.54
CDD [49]	0.68	16.23	2437.54	0.44	0.60	230.35	CDD [49]	0.69	13.04	4035.47	0.37	0.52	501.84
LRR [13]	0.59	16.61	2039.84	0.33	0.51	613.42	LRR [13]	0.70	14.48	2722.86	0.36	0.53	678.53
TarD [15]	0.46	16.99	1941.00	0.34	0.46	2342.74	TarD [15]	0.68	13.74	3385.62	0.39	0.44	1271.50
IGN [14]	0.56	17.22	1811.24	0.32	0.65	903.80	IGN [14]	0.58	12.11	4649.93	0.24	0.52	1020.07
Sup [30]	0.50	14.05	4717.51	0.24	0.27	1667.85	Sup [30]	0.69	12.98	4019.42	0.40	0.47	598.91
DIV [33]	0.34	8.51	9613.72	0.18	0.57	1364.19	DIV [33]	0.59	12.30	3957.61	0.23	0.54	871.24
TSJNet	0.69	18.13	1502.60	0.45	0.62	344.20	TSJNet	0.70	14.63	2714.86	0.33	0.53	524.41

RoadScene [41] IVIF dataset							LLVIP [10] IVIF dataset						
Method	SSIM \uparrow	PSNR \uparrow	MSE \downarrow	VIF \uparrow	CC \uparrow	CV \downarrow	Method	SSIM \uparrow	PSNR \uparrow	MSE \downarrow	VIF \uparrow	CC \uparrow	CV \downarrow
ReC [8]	0.72	15.40	2404.92	0.32	0.62	460.00	ReC [8]	0.42	14.64	2281.86	0.30	0.69	302.05
CDD [49]	0.67	14.03	3077.02	0.25	0.63	426.30	CDD [49]	0.64	14.58	2315.02	0.41	0.68	332.29
LRR [13]	0.58	11.82	4401.71	0.24	0.62	629.70	LRR [13]	0.59	15.93	1688.62	0.39	0.68	580.90
TarD [15]	0.69	14.82	2603.71	0.31	0.58	1255.83	TarD [15]	0.56	14.33	2508.97	0.41	0.65	1095.24
IGN [14]	0.52	10.31	6693.45	0.28	0.60	1033.15	IGN [14]	0.55	14.97	2137.50	0.24	0.68	638.59
Sup [30]	0.74	14.51	2928.35	0.34	0.60	420.00	Sup [30]	0.64	14.62	2306.66	0.38	0.68	360.89
DIV [33]	0.61	13.86	3033.92	0.19	0.62	907.78	DIV [33]	0.46	10.44	6362.27	0.25	0.68	645.38
TSJNet	0.70	14.52	2544.58	0.33	0.64	516.82	TSJNet	0.64	15.97	1697.69	0.37	0.67	457.46

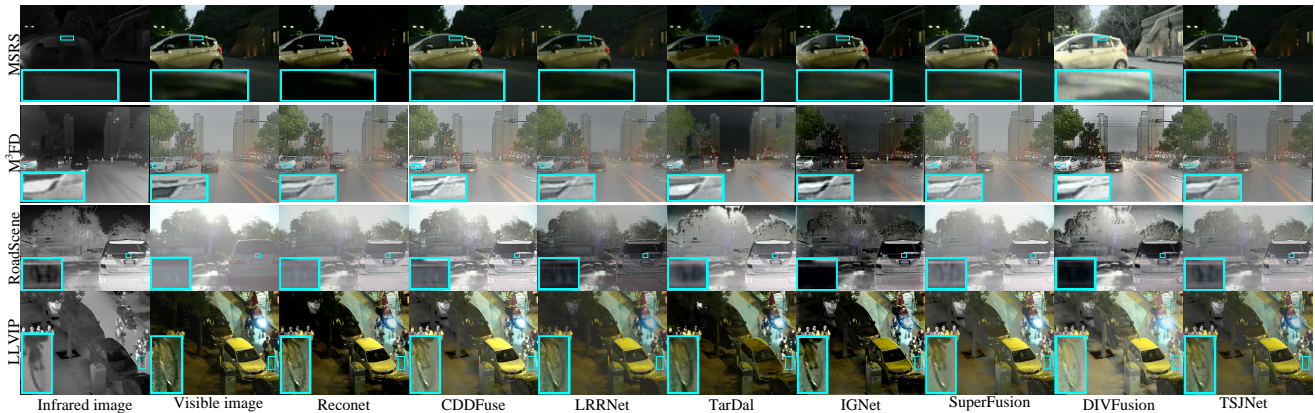


Figure 4. Subjective comparisons of different methods on MSRS, M³FD, RoadScene, and LLVIP datasets.

not conducive to conducting experiments on downstream tasks. Therefore, we provide these two kinds of labels for the four datasets with YOLO-v7 [37] and the Segment-anything model [11], which will be open-source in GitHub.

Metrics: structural similarity (SSIM), mean squared error (MSE), peak signal-to-noise ratio (PSNR), fidelity of visual information (VIF) [28], correlation coefficient (CC) [6], and Chen-Varshney metric (CV) [17].

Compared approaches: Seven SOTA approaches were selected to compare with the TSJNet: Reonet (Rec) [8], CDDFuse (CDD) [49], LRRNet (LRR) [13], TarDal (TarD) [15], IGNet (IGN) [14], SuperFusion (Sup) [30], and DIV-Fusion (DIV) [33].

5.2. Assessments of multi-modality image fusion

Subjective Comparisons. In Fig. 4, we present the subjective outcomes for the MSRS, M³FD, RoadScene, and LLVIP datasets. Clearly, the images fused by TSJNet surpassed those fused by the other SOTA methods. First, the objects of the TSJNet are distinctly accentuated, making it difficult to differentiate foreground targets from the background in darker or overexposed regions. Second, TSJNet preserves abundant edge and texture information that may be obscured by poor lighting, such as car door frames, front center nets, logos, and bike wheels.

Objective Comparisons. Table 1 lists the mean scores of six metrics for the four datasets. In general, the objective results outperformed those of the other methods. Specifically, the SSIM, CC, and MSE scored the highest overall,

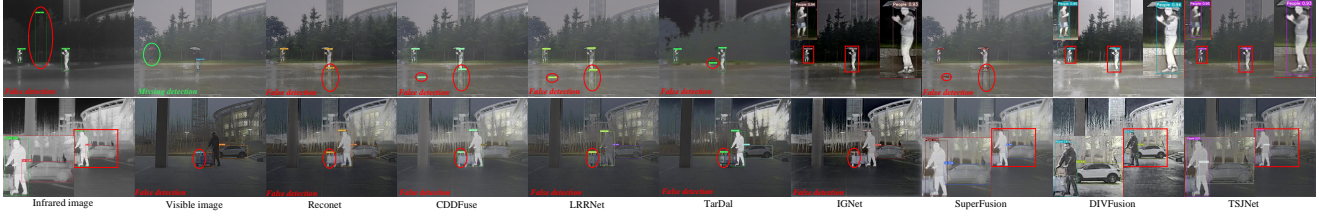


Figure 5. Detection results of different methods on M³FD dataset.

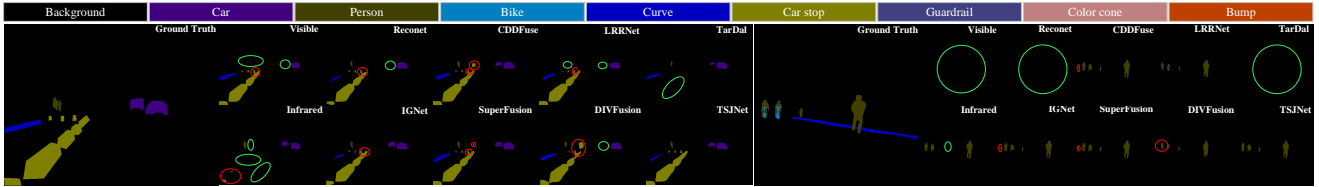


Figure 6. Segmentation results of different methods on MSRS dataset. Missing and incorrect parts are marked with green and red ovals.

demonstrating that TSJNet has a stronger resemblance to the source images. A higher PSNR value indicates that the proposed method yields lower disruption levels. As TSJNet focuses on cross-modal feature extraction, the VIF value is maintained at an elevated level. Furthermore, the better performance of CV shows that local details such as edges are well preserved by TSJNet.

5.3. Downstream applications

5.3.1 Object detection

Setup: We performed object detection on M³FD dataset, employed detector YOLO v7 [37], and evaluated the detection performance by the mean average precision (mAP) calculated at an intersection over union (IoU) of 0.5 metric (mAP@0.5). The training epoch, batch size, and initial learning rate were set to 300, 16, and 0.01, respectively.

Subjective analysis. As shown in Table 2, the values of AP@0.5 and mAP@0.5 of the fusion results were higher than those of the unfused unimodal images. CDDFuse, LRRNet, and TSJNet exhibited good detection performances. Notably, TSJNet outperformed the comparison method by 2.84% in terms of detection performance.

Objective analysis. As shown in Fig. 5, the detection results of the fused images containing complementary modal image features were generally better than those of the unimodal images. However, the fusion performances of different methods have different degrees of influence on detection accuracy. Reconet, CDDFuse, LRRNet, and TarDal misdetect the “reflection of a person” and the “bucket” as a “person.” IGNet and SuperFusion suffer from detection errors and low confidence values. The fusion result of the TSJNet contains rich target features; therefore, it effectively avoids the aforementioned problems with good confidence.

5.3.2 Semantic segmentation

Setup: We used BiSeNet [43] to segment the semantic information of nine object classes of the MSRS dataset, i.e., background, bump, color cone, guardrail, curve, bike, person, car stop, and car. The model’s effectiveness was assessed by IoU. The number of training epochs was set to 200, the batch size was eight, and the remaining parameters remained unchanged, as in the initial experiment [43].

Subjective analysis. Fig. 6 shows the segmentation results for “00939” and “00770” of MSRS. In the left example, the “yellow cones” cannot be segmented accurately, and Reconet, LRRNet, and DIVFusion cannot segment the distant cars. In the example on the right, Reconet and TarDal cannot segment the semantic information because less semantic information is contained in the image, and CDDFuse, IGNet, SuperFusion, and DIVFusion demonstrate small errors in segmenting the people at the edge position.

Objective analysis. Table 2 clearly demonstrates the segmentation superiority of TSJNet. The value of mIoU is the highest among the compared methods. Compared with its close competitors, CDDFuse and SuperFusion, TSJNet achieved higher scores in many important categories, such as curves and car stops. Furthermore, TSJNet exceeds other methods by 7.47% on the segmentation ability, which highlights the strong capabilities of our model in handling complex and detail-rich scenes.

5.4. Ablation studies

Ablation studies were conducted using the MSRS dataset. Table 3 summarizes the ablation results.

Ablation on the proposed DSM. The DSM plays a vital role in exploring local deep features across images of different modalities. From Fig. 7, the image fused without the

Table 2. Comparison of TSJNet with seven methods for semantic segmentation on the MSRS and object detection on the M³FD. The top three values are marked in red, green, and blue.

Method	IoU (Dataset: MSRS [32])										AP@0.5 (Dataset: M ³ FD) [15]						
	Background	Car	Person	Bike	Curve	Car Stop	Guardrail	Color Tone	Bump	mIoU	Peo	Car	Bus	Mot	Lam	Tru	mAP@.5
Visible	97.92	86.79	39.97	70.50	53.33	71.85	85.90	65.44	79.16	0.7232	0.803	0.912	0.946	0.841	0.667	0.890	0.843
Infrared	96.14	61.90	70.00	24.46	33.64	20.67	0.00	20.98	27.97	0.3953	0.777	0.733	0.597	0.113	0.519	0.611	0.558
ReC [8]	97.57	83.08	56.20	58.06	37.91	57.34	77.66	55.83	59.68	0.6481	0.803	0.912	0.946	0.841	0.667	0.890	0.843
CDD [49]	97.64	90.28	72.37	72.06	63.32	73.27	82.05	64.34	80.57	0.7732	0.832	0.916	0.953	0.844	0.705	0.882	0.855
LRR [13]	98.31	88.85	67.21	69.56	52.12	71.51	81.07	63.93	77.63	0.7446	0.796	0.923	0.955	0.866	0.721	0.899	0.860
TarD [15]	97.52	82.12	55.17	63.56	38.83	63.94	58.58	53.15	45.89	0.6208	0.826	0.897	0.918	0.749	0.679	0.874	0.824
IGN [14]	98.46	89.48	74.01	70.76	57.69	73.62	83.59	64.24	72.96	0.7609	0.849	0.894	0.917	0.750	0.650	0.866	0.821
Sup [30]	96.43	88.24	73.21	72.22	62.77	73.20	82.25	65.18	80.15	0.7709	0.837	0.910	0.932	0.774	0.700	0.858	0.835
DIV [33]	98.05	87.38	64.63	67.02	50.63	69.43	78.37	61.47	44.38	0.6904	0.726	0.898	0.925	0.792	0.638	0.887	0.811
TSJNet	98.55	89.97	73.73	71.32	63.59	73.90	82.71	64.69	77.48	0.7733	0.818	0.918	0.956	0.868	0.704	0.893	0.860

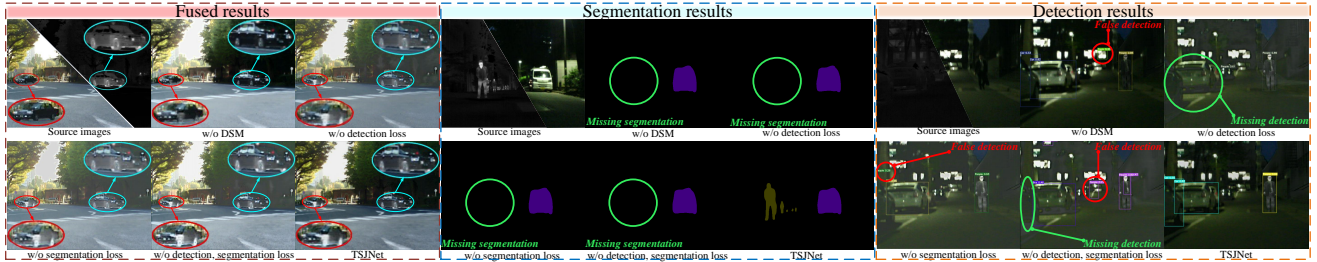


Figure 7. Subjective ablation comparisons of the DSM, detection loss and segmentation loss.

DSM has a limited ability for local brightness information extraction, *e.g.*, the tires of a car.

Ablation on detection and segmentation loss. To verify the effectiveness of detecting and segmenting double losses, we removed them separately and jointly from TSJNet, leaving the other parts unchanged. As shown in Table 3, regardless of the type of loss removal, there is an overall downward trend in the metric values. As shown in Fig. 7 rich semantic and target information are extracted using dual loss. Thus, images fused with cross-modal information concurrently achieved both robust detection and precise segmentation results. Employing detection and segmentation losses established a mutually advantageous relationship between fusion and high-level tasks.

Table 3. Results of ablation experiments in the test of MSRS

Method	SSIM \uparrow	PSNR \uparrow	MSE \downarrow	CC \uparrow	CV \downarrow
w/o DSM	0.66	14.83	3731.88	0.54	560.46
w/o \mathcal{L}_{Det}	0.55	14.86	2550.33	0.54	376.49
w/o \mathcal{L}_{Seg}	0.50	12.46	4167.93	0.60	464.51
w/o $\mathcal{L}_{Det, Seg}$	0.49	12.43	4246.27	0.51	363.24
TSJNet	0.69	18.13	1502.60	0.62	344.20

6. Conclusion

In this paper, we propose a target and semantic awareness joint-driven fusion network. With the assistance of autoencoder structure and well-designed DSM, we fully extract

cross-modal independent modal features and incorporate detection loss and segmentation loss into the fusion network. Notably, experiments demonstrate that TSJNet focuses not only on enhancing image details, but also on capturing high-level semantic and target information, thus facilitating downstream tasks. In the future, we will explore a more lightweight and effective fusion network to better implement its applications in automated driving and security surveillance.

7. Acknowledgment

This research was supported in part by the National Natural Science Foundation of China under Grant 62201149, in part by the Guangdong Higher Education Innovation and Strengthening of Universities Project under Grant 2023KTSCX127, and in part by the Foshan Key Areas of Scientific and Technological Research Project under Grant 2120001008558.

References

- [1] Bing Cao, Yiming Sun, Pengfei Zhu, and Qinghua Hu. Multi-modal gated mixture of local-to-global experts for dynamic image fusion. In *Proceedings of the IEEE/CVF International Conference on Computer Vision*, pages 23555–23564, 2023. 2
- [2] Dongliang Chang, Yujun Tong, Ruoyi Du, Timothy Hospedales, Yi-Zhe Song, and Zhanyu Ma. An erudite fine-grained visual classification model. In *Proceedings of*

- the *IEEE/CVF Conference on Computer Vision and Pattern Recognition*, pages 7268–7277, 2023. 5
- [3] Hanting Chen, Yunhe Wang, Tianyu Guo, Chang Xu, Yiping Deng, Zhenhua Liu, Siwei Ma, Chunjing Xu, Chao Xu, and Wen Gao. Pre-trained image processing transformer. In *2021 IEEE/CVF Conference on Computer Vision and Pattern Recognition (CVPR)*, 2021. 2
- [4] Liang-Chieh Chen, George Papandreou, Florian Schroff, and Hartwig Adam. Rethinking atrous convolution for semantic image segmentation. *arXiv preprint arXiv:1706.05587*, 2017. 3, 5
- [5] Yuanshen Guan, Ruikang Xu, Mingde Yao, Lizhi Wang, and Zhiwei Xiong. Mutual-guided dynamic network for image fusion. In *Proceedings of the 31st ACM International Conference on Multimedia*, pages 1779–1788, 2023. 2
- [6] Z. Han, X. Tang, X. Gao, and F. Hu. Image fusion and image quality assessment of fused images. *The International Archives of the Photogrammetry, Remote Sensing and Spatial Information Sciences*, XL-7/W1:33–36, 2013. 6
- [7] Ali Hassani, Steven Walton, Jiachen Li, Shen Li, and Humphrey Shi. Neighborhood attention transformer. In *Proceedings of the IEEE/CVF Conference on Computer Vision and Pattern Recognition*, pages 6185–6194, 2023. 3
- [8] Zhanbo Huang, Jinyuan Liu, Xin Fan, Risheng Liu, Wei Zhong, and Zhongxuan Luo. Reconet: Recurrent correction network for fast and efficient multi-modality image fusion. In *European Conference on Computer Vision*, pages 539–555. Springer, 2022. 6, 8
- [9] Ida Häggström, C. Ross Schmidtlein, Gabriele Campanella, and Thomas J. Fuchs. Deeppet: A deep encoder-decoder network for directly solving the pet image reconstruction inverse problem. *Medical Image Analysis*, page 253–262, 2019. 2
- [10] Xinyu Jia, Chuang Zhu, Minzhen Li, Wenqi Tang, and Wenli Zhou. Lvip: A visible-infrared paired dataset for low-light vision. In *2021 IEEE/CVF International Conference on Computer Vision Workshops (ICCVW)*, 2021. 5, 6
- [11] Alexander Kirillov, Eric Mintun, Nikhila Ravi, Hanzi Mao, Chloe Rolland, Laura Gustafson, Tete Xiao, Spencer Whitehead, AlexanderC Berg, Wan-Yen Lo, Piotr Dollár, and Ross Girshick. Segment anything. 6
- [12] Hui Li, Xiao-Jun Wu, and Josef Kittler. Rfn-nest: An end-to-end residual fusion network for infrared and visible images. *Information Fusion*, page 72–86, 2021. 2
- [13] Hui Li, Tianyang Xu, Xiao-Jun Wu, Jiwen Lu, and Josef Kittler. Lrnet: A novel representation learning guided fusion network for infrared and visible images. *IEEE transactions on pattern analysis and machine intelligence*, 2023. 6, 8
- [14] Jiawei Li, Jiansheng Chen, Jinyuan Liu, and Huimin Ma. Learning a graph neural network with cross modality interaction for image fusion. In *Proceedings of the 31st ACM International Conference on Multimedia*, pages 4471–4479, 2023. 2, 4, 6, 8
- [15] Jinyuan Liu, Xin Fan, Zhanbo Huang, Guanyao Wu, Risheng Liu, Wei Zhong, and Zhongxuan Luo. Target-aware dual adversarial learning and a multi-scenario multi-modality benchmark to fuse infrared and visible for object detection. In *Proceedings of the IEEE/CVF Conference on Computer Vision and Pattern Recognition*, pages 5802–5811, 2022. 1, 2, 5, 6, 8
- [16] Jinyuan Liu, Zhu Liu, Guanyao Wu, Long Ma, Risheng Liu, Wei Zhong, Zhongxuan Luo, and Xin Fan. Multi-interactive feature learning and a full-time multi-modality benchmark for image fusion and segmentation. In *Proceedings of the IEEE/CVF international conference on computer vision*, pages 8115–8124, 2023. 2
- [17] Z. Liu, E. Blasch, Z. Xue, J. Zhao, R. Laganier, and W. Wu. Objective assessment of multiresolution image fusion algorithms for context enhancement in night vision: A comparative study. *IEEE Transactions on Pattern Analysis and Machine Intelligence*, page 94–109, 2012. 6
- [18] Ze Liu, Yutong Lin, Yue Cao, Han Hu, Yixuan Wei, Zheng Zhang, Stephen Lin, and Baining Guo. Swin transformer: Hierarchical vision transformer using shifted windows. In *2021 IEEE/CVF International Conference on Computer Vision (ICCV)*, 2021. 4
- [19] Zhu Liu, Jinyuan Liu, Guanyao Wu, Long Ma, Xin Fan, and Risheng Liu. Bi-level dynamic learning for jointly multi-modality image fusion and beyond. *arXiv preprint arXiv:2305.06720*, 2023. 2
- [20] Jiayi Ma, Han Xu, Junjun Jiang, Xiaoguang Mei, and Xiaoping Zhang. Ddcgan: A dual-discriminator conditional generative adversarial network for multi-resolution image fusion. *IEEE Transactions on Image Processing*, page 4980–4995, 2020. 2
- [21] Jiayi Ma, Hao Zhang, Zhenfeng Shao, Pengwei Liang, and Han Xu. Ganmcc: A generative adversarial network with multiclassification constraints for infrared and visible image fusion. *IEEE Transactions on Instrumentation and Measurement*, 70:1–14, 2020. 2
- [22] Jiayi Ma, Linfeng Tang, Fan Fan, Jun Huang, Xiaoguang Mei, and Yong Ma. Swinfusion: Cross-domain long-range learning for general image fusion via swin transformer. *IEEE/CAA Journal of Automatica Sinica*, 9(7):1200–1217, 2022. 2, 3
- [23] Paulius Micikevicius, Sharan Narang, JonahM. Alben, Gregory Diamos, Erich Elsen, David Garcia, Boris Ginsburg, MichaelJ. Houston, Oleksii Kuchaiev, Ganesh Venkatesh, and Hao Wu. Mixed precision training. *International Conference on Learning Representations, International Conference on Learning Representations*, 2017. 5
- [24] Linhao Qu, Shaolei Liu, Manning Wang, and Zhijian Song. Transmef: A transformer-based multi-exposure image fusion framework using self-supervised multi-task learning. In *Proceedings of the AAAI conference on artificial intelligence*, pages 2126–2134, 2022. 2
- [25] Prajit Ramachandran, Niki Parmar, Ashish Vaswani, Irwan Bello, Anselm Levskaya, and Jonathon Shlens. Stand-alone self-attention in vision models. *arXiv: Computer Vision and Pattern Recognition, arXiv: Computer Vision and Pattern Recognition*, 2019. 4
- [26] Dongyu Rao, Tianyang Xu, and Xiao-Jun Wu. Tgfuse: An infrared and visible image fusion approach based on transformer and generative adversarial network. *IEEE Transactions on Image Processing*, 2023. 2

- [27] Shaoqing Ren, Kaiming He, Ross Girshick, and Jian Sun. Faster r-cnn: Towards real-time object detection with region proposal networks. *IEEE Transactions on Pattern Analysis and Machine Intelligence*, page 1137–1149, 2017. 3, 4, 5
- [28] H.R. Sheikh and A.C. Bovik. Image information and visual quality. In *2004 IEEE International Conference on Acoustics, Speech, and Signal Processing*, 2004. 6
- [29] Yiming Sun, Bing Cao, Pengfei Zhu, and Qinghua Hu. Det-fusion: A detection-driven infrared and visible image fusion network. In *Proceedings of the 30th ACM International Conference on Multimedia*, pages 4003–4011, 2022. 1, 2, 5
- [30] Linfeng Tang, Yuxin Deng, Yong Ma, Jun Huang, and Jiayi Ma. Superfusion: A versatile image registration and fusion network with semantic awareness. *IEEE/CAA Journal of Automatica Sinica*, page 2121–2137, 2022. 6, 8
- [31] Linfeng Tang, Jiteng Yuan, and Jiayi Ma. Image fusion in the loop of high-level vision tasks: A semantic-aware real-time infrared and visible image fusion network. *Information Fusion*, page 28–42, 2022. 1, 2
- [32] Linfeng Tang, Jiteng Yuan, Hao Zhang, Xingyu Jiang, and Jiayi Ma. Piafusion: A progressive infrared and visible image fusion network based on illumination aware. *Information Fusion*, 83:79–92, 2022. 1, 5, 6, 8
- [33] Linfeng Tang, Xinyu Xiang, Hao Zhang, Meiqi Gong, and Jiayi Ma. Divfusion: Darkness-free infrared and visible image fusion. *Information Fusion*, 91:477–493, 2023. 6, 8
- [34] Linfeng Tang, Hao Zhang, Han Xu, and Jiayi Ma. Rethinking the necessity of image fusion in high-level vision tasks: A practical infrared and visible image fusion network based on progressive semantic injection and scene fidelity. *Information Fusion*, page 101870, 2023. 2
- [35] Wei Tang, Fazhi He, and Yu Liu. Ydtr: Infrared and visible image fusion via y-shape dynamic transformer. *IEEE Transactions on Multimedia*, page 1–16, 2022. 3
- [36] Ashish Vaswani, Noam Shazeer, Niki Parmar, Jakob Uszkoreit, Llion Jones, Aidan N. Gomez, Lukasz Kaiser, and Illia Polosukhin. Attention is all you need. *Neural Information Processing Systems, Neural Information Processing Systems*, 2017. 2
- [37] Chien-Yao Wang, Alexey Bochkovskiy, and Hong-Yuan Mark Liao. Yolov7: Trainable bag-of-freebies sets new state-of-the-art for real-time object detectors. In *Proceedings of the IEEE/CVF Conference on Computer Vision and Pattern Recognition*, pages 7464–7475, 2023. 6, 7
- [38] Di Wang, Jinyuan Liu, Xin Fan, and Risheng Liu. Unsupervised misaligned infrared and visible image fusion via cross-modality image generation and registration. *arXiv preprint arXiv:2205.11876*, 2022. 2
- [39] Di Wang, Jinyuan Liu, Risheng Liu, and Xin Fan. An interactively reinforced paradigm for joint infrared-visible image fusion and saliency object detection. *Information Fusion*, 98:101828, 2023. 2
- [40] Wanxin Xiao, Yafei Zhang, Hongbin Wang, Fan Li, and Hua Jin. Heterogeneous knowledge distillation for simultaneous infrared-visible image fusion and super-resolution. *IEEE Transactions on Instrumentation and Measurement*, 71:1–15, 2022. 2
- [41] Han Xu, Jiayi Ma, Zhuliang Le, Junjun Jiang, and Xiaojie Guo. FusionDn: A unified densely connected network for image fusion. *Proceedings of the AAAI Conference on Artificial Intelligence*, page 12484–12491, 2020. 5, 6
- [42] Han Xu, Jiayi Ma, Jiteng Yuan, Zhuliang Le, and Wei Liu. Rfnet: Unsupervised network for mutually reinforcing multi-modal image registration and fusion. In *Proceedings of the IEEE/CVF conference on computer vision and pattern recognition*, pages 19679–19688, 2022. 2, 3
- [43] Changqian Yu, Jingbo Wang, Chao Peng, Changxin Gao, Gang Yu, and Nong Sang. BiSeNet: Bilateral Segmentation Network for Real-time Semantic Segmentation, page 334–349. 2018. 7
- [44] Jun Yue, Leyuan Fang, Shaobo Xia, Yue Deng, and Jiayi Ma. Dif-fusion: Towards high color fidelity in infrared and visible image fusion with diffusion models. *arXiv preprint arXiv:2301.08072*, 2023. 2
- [45] Hao Zhang, Han Xu, Yang Xiao, Xiaojie Guo, and Jiayi Ma. Rethinking the image fusion: A fast unified image fusion network based on proportional maintenance of gradient and intensity. *Proceedings of the AAAI Conference on Artificial Intelligence*, page 12797–12804, 2020. 2
- [46] Hang Zhang, Chongruo Wu, Zhongyue Zhang, Yi Zhu, Haibin Lin, Zhi Zhang, Yue Sun, Tong He, Jonas Mueller, R Manmatha, et al. Resnest: Split-attention networks. In *Proceedings of the IEEE/CVF conference on computer vision and pattern recognition*, pages 2736–2746, 2022. 2
- [47] Jun Zhang, Licheng Jiao, Wenping Ma, Fang Liu, Xu Liu, Lingling Li, Puhua Chen, and Shuyuan Yang. Transformer based conditional gan for multimodal image fusion. *IEEE Transactions on Multimedia*, page 1–14, 2023. 1, 2
- [48] Wenda Zhao, Shigeng Xie, Fan Zhao, You He, and Huchuan Lu. Metafusion: Infrared and visible image fusion via meta-feature embedding from object detection. In *Proceedings of the IEEE/CVF Conference on Computer Vision and Pattern Recognition*, pages 13955–13965, 2023. 2
- [49] Zixiang Zhao, Haowen Bai, Jianshe Zhang, Yulun Zhang, Shuang Xu, Zudi Lin, Radu Timofte, and Luc Van Gool. Cddfuse: Correlation-driven dual-branch feature decomposition for multi-modality image fusion. In *Proceedings of the IEEE/CVF Conference on Computer Vision and Pattern Recognition*, pages 5906–5916, 2023. 2, 3, 6, 8
- [50] Zixiang Zhao, Haowen Bai, Yuanzhi Zhu, Jianshe Zhang, Shuang Xu, Yulun Zhang, Kai Zhang, Deyu Meng, Radu Timofte, and LucVan Gool. Ddfm: Denoising diffusion model for multi-modality image fusion. *Accepted by ICCV 2023 (Oral)*, 2023. 2